

# Friction and Delamination Properties of Self-Mating Diamond-Like Carbon Coatings in Water

Yasunori Niiyama<sup>1</sup> · Naotoshi Shimizu<sup>2</sup> · Akinori Kuwayama<sup>1</sup> · Hiroshi Okada<sup>1</sup> · Takanori Takeno<sup>2</sup> · Kazue Kurihara<sup>3</sup> · Koshi Adachi<sup>2</sup>

Received: 30 November 2015 / Accepted: 1 April 2016 / Published online: 13 April 2016  
© Springer Science+Business Media New York 2016

**Abstract** The friction and delamination properties of self-mating diamond-like carbon (DLC) coatings in water and ambient air were investigated using a ball-on-disk tribometer. An a-C:H-type DLC coating was deposited on SUJ2 bearing steel using plasma chemical vapor deposition. Delamination of DLC coatings occurred in water in relatively mild contact conditions, such as applying a low load and a high sliding speed. However, no delamination occurred under severe contact conditions. Furthermore, delamination never occurred under ambient air conditions. The process that prevents delamination occurring under ambient air conditions is clarified using a detailed analysis of SEM data. Micro-cracks were caused by Hertzian contact with droplets, which then propagated into large ruptures under water conditions; however, they disappeared and formed a smooth surface under ambient air conditions. This is because of the structural change to an  $sp^2$ -rich surface. Enhancement of the structural change of DLC coating could suppress delamination in water.

**Keywords** Diamond-like carbon · Coating · Tribology · Delamination · Water · Friction

## 1 Introduction

Waste heat recovery is a promising technology that contributes to energy conservation as well as reducing friction loss in various mechanical systems and energy conversion systems. Specifically, water lubrication technology is essential for the waste heat generation system because it uses water as a working fluid [1]. Diamond-like carbon (DLC) coatings have good tribological properties, including surface flatness, high hardness, high wear resistance, low friction and chemical inertness [2]. However, it is reported that the delamination of DLC coatings occurs in wet conditions, despite the lower friction present compared with ambient air conditions [3, 4]. Ohana et al. proposed that the delamination mechanism of DLC coatings results from water permeating into micro-cracks caused by contact stress and that the delamination-resistant DLC coating can be improved by adding a top layer of Si-doped DLC [5, 6]. However, this mechanism remains uncertain because the delamination process was not clearly observed. Moreover, the experiments did not satisfy the design guidelines of DLC water lubrication because of a lack of wide-ranging experimental conditions.

From a practical perspective, to use DLC coatings for water lubrication, it is essential to suppress the delamination under several operating conditions. Therefore, the conditions and the process of delamination occurrence or suppression can be revealed by investigating the friction and delamination properties of mating DLC coatings in water, using a ball-on-disk tribometer, which this paper presents. Furthermore, the required conditions to suppress delamination are clarified following a detailed analysis of SEM, Raman spectroscopy and nanoindentation data. It is beneficial for the practical use of DLC coatings to clarify the friction and delamination properties in water.

✉ Yasunori Niiyama  
yasunori\_niiyama@denso.co.jp

<sup>1</sup> Corporate R&D Division 2, DENSO CORPORATION, 1-1, Showa-cho, Kariya 448-8661, Japan

<sup>2</sup> Department of Nanomechanics, Graduate School of Engineering, Tohoku University, 6-6-1, Aoba, Aramaki, Aoba-ku, Sendai 980-8579, Japan

<sup>3</sup> WPI-Advanced Institute for Materials Research and Institute of Multidisciplinary Research for Advanced Materials, Tohoku University, 2-1-1 Katahira, Aoba-ku, Sendai 980-8577, Japan

## 2 Experimental Procedure

### 2.1 Experimental Apparatus

Figure 1 shows a schematic illustration of the experimental setup of the ball-on-disk-type tribometer used in this research. A ball specimen was fixed in a ball holder attached in front of an arm. A disk specimen, supported in the end-of-motor axis, was rotated directly by a motor. The ball was pressed onto the disk by a weight on the opposite side of the ball, via a pivot, that a normal load could be applied in the contact point. For experiments carried out under water conditions, the ball and disk were submerged in a bath filled with temperature-controlled purified water. This allowed the contact point of the ball on the disk to be wetted. The normal load varied between 1 and 20 N and was calibrated using a load cell prior to the experiment. The friction force was also determined by a load cell. The sliding speed was controlled by the motor rotation speed and varied between 0.01 and 1 m/s. The ball holder was removable and could be positioned with micrometer accuracy by tapered pins. Therefore, the friction test could be restarted at approximately the same contact point by observing the wear scar on the ball. The wear scar on the ball was detected and measured using a confocal microscope (Lasertec OPTELICS H1200) and a scanning electron microscope (SEM, Hitachi High-Tech-science SU8020) to investigate the change in the wear scar and delamination process.

### 2.2 Specimens

DLC coatings were deposited on a SUJ2 bearing steel ball with a diameter of 8 mm, and on a SUJ2 bearing steel disk specimen with a diameter of 30 mm and a thickness of approximately 3 mm, using plasma chemical vapor deposition (CVD) made by Tohken Thermo Tech Co., Ltd. The DLC coatings were a-C:H type with a hydrogen content of 25 %, a Vickers hardness of 2250 and a Young's modulus

of 215 GPa, which were measured using the nanoindentation method (Elionix, ENT2100). The CVD source gas was acetylene. An intermediate layer was formed by the graded layer of W and W-doped DLC, with a thickness of approximately 0.7  $\mu\text{m}$ . The ball and disk specimens had a similar surface roughness of 25 nm Rq and 20 nm Rq, respectively.

### 2.3 Raman Spectra

Raman spectroscopy (Tokyo Instruments, Inc., Nanofinder30) was carried out to investigate the structural change of DLC in the ball surface. The laser wavelength used was 532 nm, and the laser power was 5 mW. The exposure time was 1 s, and 128 spectra were accumulated. Five different positions on the ball were analyzed, and all were within a 200  $\mu\text{m}$  radius from the ball contact center.

## 3 Experimental Results

### 3.1 Friction and Delamination Properties in Water

The wear mode can be classified into two types, such as forming a smooth surface and the onset of delamination. Figure 2 shows the measured coefficient of friction determined under water conditions for two different speeds (0.01 and 1 m/s) and with a constant load of 1 N. The friction was lower and more constant when the sliding speed was 1 m/s than when it was 0.01 m/s. This means that throughout whole sliding distance tested (0–1000 m) the maximum friction coefficient and the difference between the maximum and the minimum of the friction coefficient are smaller when the sliding speed is 1 m/s, rather than 0.01 m/s. However, Fig. 3a shows that a rough wear scar and exposure of the interlayer (shown as white marks), which is caused by rupture of the DLC coating, occur on the ball when the sliding speed is 1 m/s. That

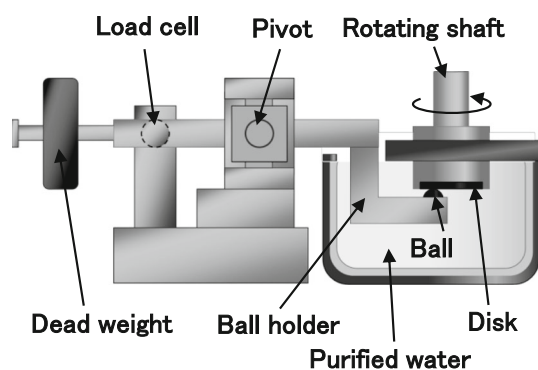


**Fig. 1** Schematic illustration of the experimental setup

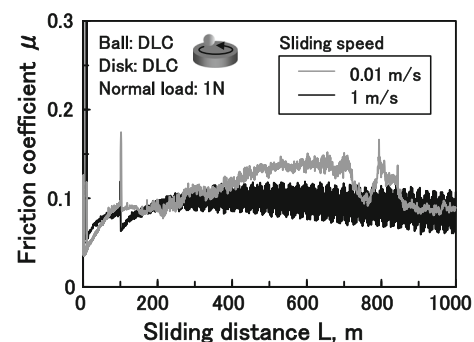


**Fig. 2** Representative friction behavior in water, with a normal load of 1 N, for two sliding speeds: 0.01 m/s and 1 m/s

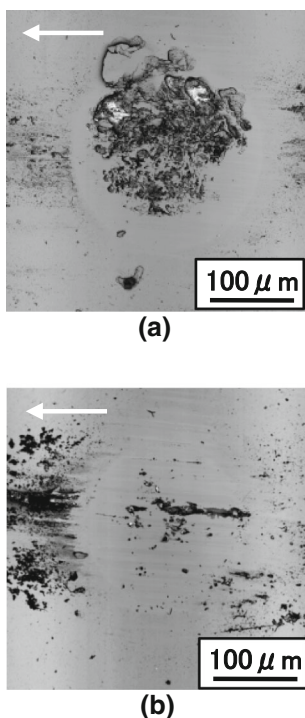


**Fig. 3** Optical image of the wear scar on the ball after sliding 1000 m in water when the sliding speed was **a** 1 m/s and **b** 0.01 m/s

phenomenon is defined as *delamination*. Conversely, a smoother wear scar was formed and delamination did not occur when the sliding speed is 0.01 m/s, as shown in Fig. 3b. The aforementioned results are interesting from a mechanical point of view because delamination occurred under the relatively lower shear stress condition.

Figure 4 shows the occurrence of delamination as functions of sliding speed and initial contact pressure, for experiments under wet conditions. The horizontal axis shows the value of  $p_i$ , which is the initial contact pressure, as an indicator of contact severity. A decrease of  $p_i$  represents mild conditions, whereas an increase of  $p_i$

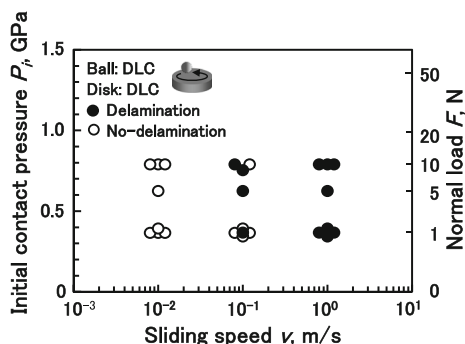


**Fig. 4** Distribution of delamination occurrence as functions of the sliding velocity and initial contact pressure, for under water conditions

represents severe conditions. Delamination occurred at relatively mild contact conditions but did not under severe contact conditions, particularly when the sliding speed was 0.01 m/s.

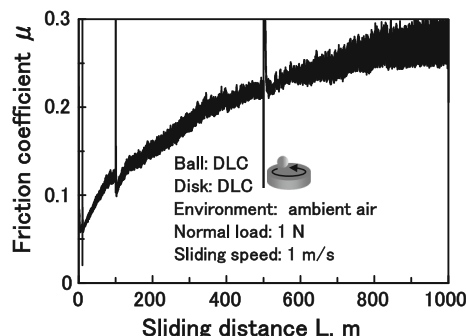
### 3.2 Friction and Delamination Properties in Ambient Air

Figure 5 shows the friction behavior in ambient air, an environment which represents a more severe contact condition because there is no fluid lubrication. The friction coefficient under ambient air conditions was approximately three times larger than that measured under water conditions. Therefore, it was concluded that each specimen is in more severe contact in ambient air. Figure 6 shows optical images of a wear scar after the friction test. Delamination and a rough surface did not occur under this condition, despite the large friction coefficient. Furthermore, delamination never occurred under any conditions in ambient air, as shown in Fig. 7. This suggests that the wear mechanisms in water and in ambient air are not the same and that the key to understand the delamination mechanism is focusing on the difference.

## 4 Discussion

### 4.1 Delamination Process

Figures 8 and 9 show detailed SEM images that demonstrate the wear process that occurred under both water and ambient air conditions, respectively, when a normal load of 1 N was applied and the sliding speed was 1 m/s. Under the water condition, fan-shaped micro-cracks with widths of 2–5  $\mu\text{m}$  were generated on the wear scar after a sliding distance of 1 m. As the sliding distance increased, several small ruptures with diameters of 5–10  $\mu\text{m}$  occurred, as a result of the propagation of micro-cracks. After a sliding distance of 50 m, medium-sized ruptures, with a height of



**Fig. 5** Friction behavior in ambient air, with a normal load 1 N, when the sliding speed is 1 m/s

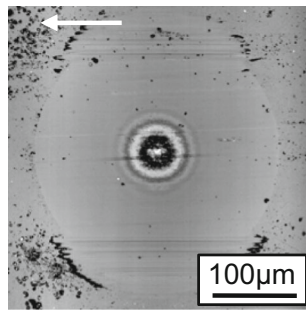


**Fig. 6** Optical image of the wear scar on the ball after sliding in ambient air

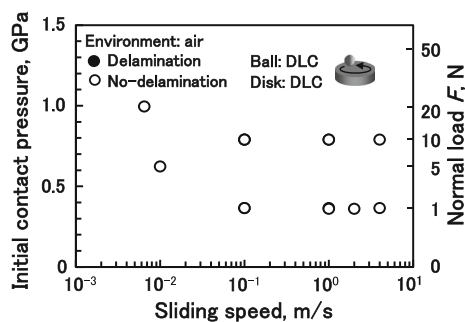


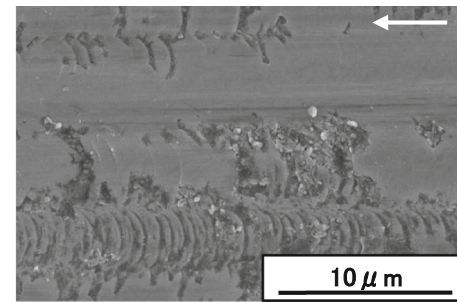
**Fig. 7** Distribution of delamination occurrence, after sliding in ambient air, as functions of the sliding velocity and initial contact pressure

10  $\mu\text{m}$  and width of 20  $\mu\text{m}$ , were formed from the combination of several smaller ruptures. This was measured by 3D cross-sectional observation using a confocal microscope's 3D scanning function. By 100 m, the interlayer was exposed as a result of a larger rupture.

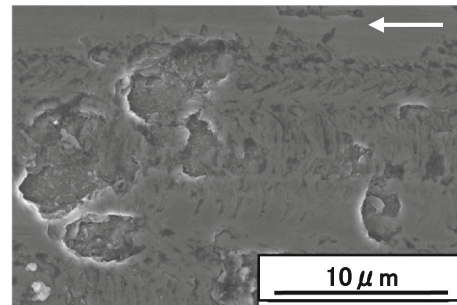
Under ambient air conditions, fan-shaped micro-cracks with widths of 2–5  $\mu\text{m}$  were also generated after a sliding distance of 1 m. However, the cracks did not propagate any further for longer sliding distances. In fact, the cracks decreased with an increase in sliding distance. Eventually, the cracks disappeared and a smooth surface was formed on the wear scar. Delamination occurs because of the propagation of cracks generated after the initial sliding process under mild contact conditions. However, under severe contact conditions delamination did not occur because the cracks generated in the initial sliding process eventually disappeared. Therefore, it is essential to control the propagation of cracks to suppress delamination.

#### 4.2 The cause of Crack Generation, Propagation and Suppression

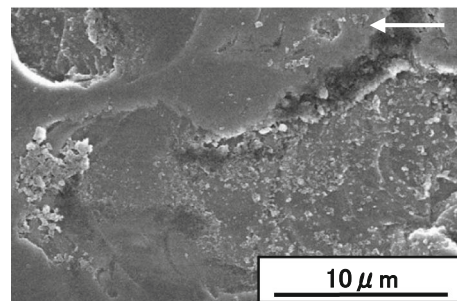
The initial cause of crack generation is considered to be a result of an increase in localized tensile stress from contact with a droplet on the disk, which is shown in Fig. 10. This



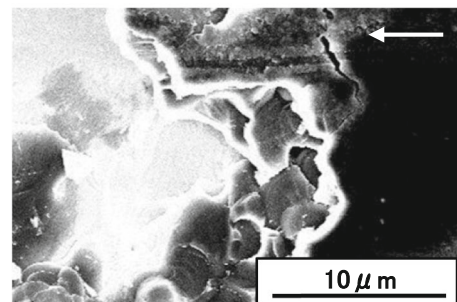
**(a)** 1m (Small cracks initiation)



**(b)** 10m (Propagation of cracks)



**(c)** 50m (Small delamination)

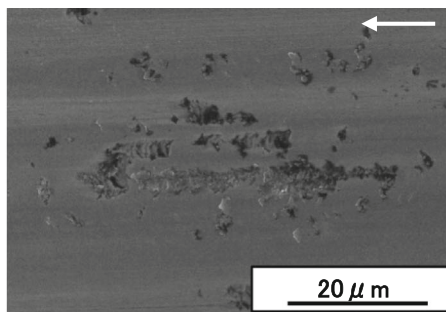


**(d)** 100m (Exposure of inter layer)

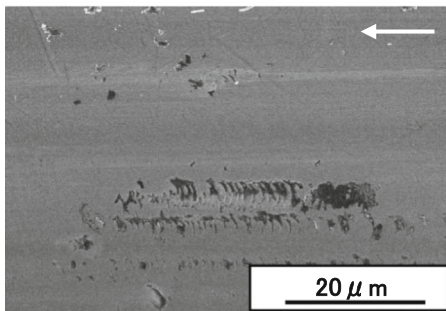
**Fig. 8** SEM images of the wear scar on the ball sliding in water, with a normal load of 1 N, when the sliding speed is 1 m/s

is the reason why the size of the droplet was similar to that of the fan-shaped cracks. Although droplets exist on the ball initially, they disappear immediately through wear. Therefore, the droplets on the initial ball surface were not responsible for the cracks. Furthermore, the maximum

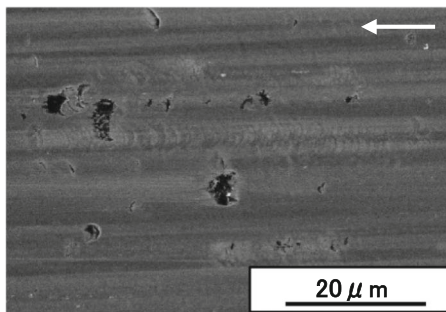




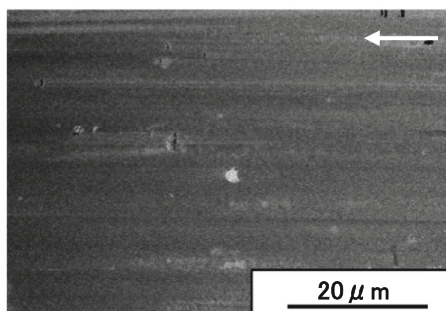
(a) 1m (Small crack initiation)



(b) 5m (Non-propagation of cracks)



(c) 10m (Decreasing of cracks)



(d) 50m (Disappearing of cracks)

**Fig. 9** SEM images of wear scar on the ball sliding in ambient air, with a normal load of 1 N, when the sliding speed is 1 m/s

tensile stress was calculated to be roughly 28 GPa, after taking into consideration the normal load and number of the droplets [7]. Therefore, it seems reasonable that crack

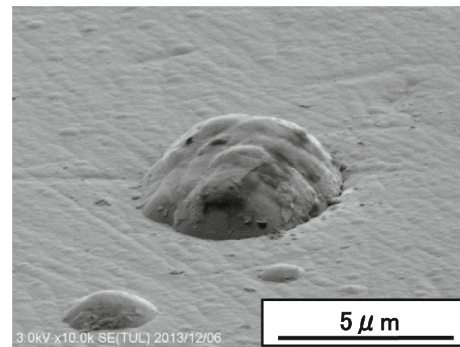


**Fig. 10** SEM image of a droplet on the disk

generation was related to the droplets on the disk. To discuss the difference in the delamination process for the different conditions, histograms of the droplet heights before and after the friction test were compared. Figure 11 presents these histograms and shows the number of droplets found in an area of 180 μm × 180 μm. Under both

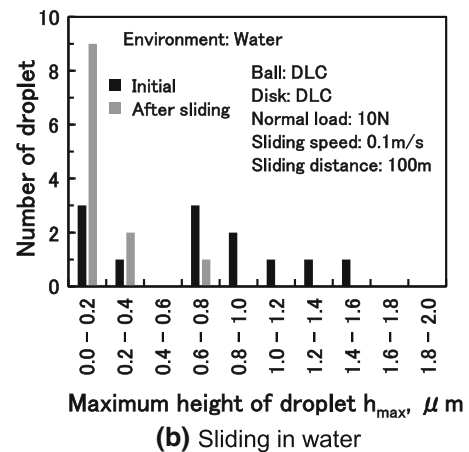
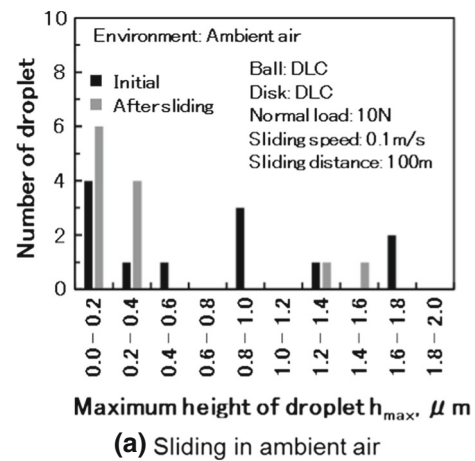


**Fig. 11** Histogram showing the maximum height of droplets before and after the friction test under each condition: in ambient air (a) and in water (b)

ambient air and water conditions, the height of the droplets decreased after the friction test. However, relatively tall droplets were present in the ambient air condition where delamination never occurred. It is suggested that the presence of the droplet alone cannot affect the delamination.

To investigate the influence of the structural change of DLC caused by friction on the delamination processes, the initial surface and wear scar of the ball were analyzed using Raman spectroscopy. In this research, the *G*-position, which represents the Raman shift of the *G*-band peak position, was adopted as an indicator of the structural change of DLC. It was reported that the *G*-position has a relationship with the fraction of  $sp^2$  hybridization in DLC, and that the *G*-position shifts to a higher wave number as the  $sp^2$  fraction increases [8, 9]. Figure 12 shows that the *G*-position of the worn surface, after sliding in ambient air conditions, shifted to a greater wave number than for the surface after sliding in water conditions. It is proposed that the increase in the  $sp^2$  fraction indicates graphitization as a result of sliding in ambient air, as reported in previous studies [10, 11]. To verify the above results, the hardness of the initial and worn surfaces of DLC was evaluated using a nanoindenter. Figure 13 shows the relationship between the indentation hardness and the indentation depth after sliding for 314 m in ambient air with a sliding speed of 0.1 m/s and with an applied normal load of 10 N. The results of the various friction tests performed in this study suggest that delamination of DLC coatings hardly occurs under severe contact conditions. Furthermore, structural changes in the DLC under severe contact conditions are related to the suppression of delamination. To clarify this phenomenon, a 10-N load was applied because it presents a more severe condition than the 1-N load that was previously applied in the acceleration tests. The hardness of the worn surfaces, where the indentation depth was below 50 nm, was reduced from an initial 26 to 18–23 GPa. Graphitization formed as a result of sliding in ambient air. Therefore, delamination was suppressed because of an

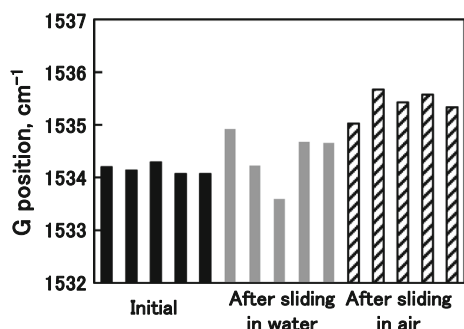


**Fig. 12** *G*-position of Raman spectra of the friction and non-friction points after sliding in water and in air

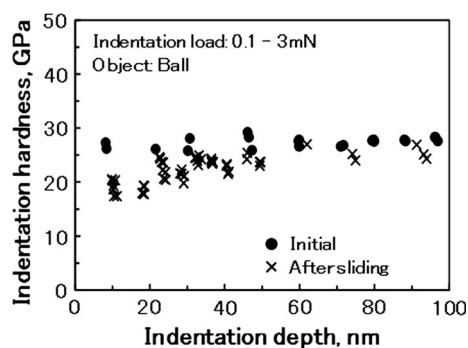


**Fig. 13** Effect of sliding in ambient air on indentation hardness on the ball as function of indentation depth

increase of the fracture toughness of the DLC surface that resulted from the graphitization.

## 5 Conclusions

In this paper the following points were revealed from investigations of the friction and delamination properties of mating DLC coatings in water and ambient air conditions.

1. Delamination occurred under relatively mild contact conditions, such as a sliding speed 1 m/s, and an applied normal load of 1, 5 and 10 N. However, no delamination occurred under the relatively severe contact conditions, such as for a sliding speed of 0.01 m/s, and an applied normal load of 1, 5 and 10 N.
2. When delamination occurred, micro-cracks were generated from contact with droplets on the disk, which propagated to form a large rupture that exposed the interlayer. However, the delamination was suppressed when micro-cracks did not propagate and instead disappeared.
3. The *G*-position of the Raman shift was determined by analyzing the worn surfaces after sliding in both the ambient air and water conditions. The *G*-position shifted to higher wave numbers for the former condition (the delamination suppression condition).
4. The indentation hardness of the surface of wear scars on the ball that were shallower than 50 nm was reduced by about 30 % of the initial surface hardness.
5. The required conditions to suppress delamination include a structural change and an increase in  $sp^2$  hybridization because this increases the fracture toughness of the DLC surface under severe friction conditions.

**Acknowledgments** This work was supported by “Tohoku Innovative Materials Technology Initiatives for Reconstruction (TIMT),” funded by the Ministry of Education, Culture, Sports, Science and Technology (MEXT) and Reconstruction Agency, Japan.

## References

1. Yatsuzuka, S., Niiyama, Y., Fukuda, K., Shikazono, N.: A liquid-piston steam engine (the design and performance evaluation of a liquid-piston steam engine). *Trans. Jpn. Soc. Mech. Eng.* **B 79**(808), 2859–2872 (2013) (in Japanese)
2. Erdemir, A., Donnet, C.: Tribology of diamond-like carbon films: recent progress and future prospects. *J. Phys. D* **39**(R311), 311–327 (2006)
3. Suzuki, M., Ohana, T., Tanaka, A.: Tribological properties of DLC films with different hydrogen contents in water environment. *Diam. Relat. Mater.* **13**(11–12), 2216–2220 (2004)
4. Zhao, F., Li, H.X., Ji, L., Mo, Y.F., Quan, W.L., Du, W., Zhou, H.D., Chen, J.M.: Superlow friction behavior of Si-doped hydrogenated amorphous carbon film in water environment. *Surf. Coat. Technol.* **203**(8), 981–985 (2009)
5. Ohana, T., Nakamura, T., Suzuki, M., Tanaka, A., Koga, Y.: Tribological properties and characterization of DLC films deposited by pulsed bias CVD. *Diam. Relat. Mater.* **13**, 1500–1504 (2004)
6. Wu, X., Suzuki, M., Ohana, T., Tanaka, A.: Characteristics and tribological properties in water of Si-DLC coatings. *Diam. Relat. Mater.* **17**, 7–12 (2008)
7. Franco Jr, A., Roberts, S.G.: Surface mechanical analyses by Hertzian indentation. *Cerâmica* **50**, 94–108 (2004)
8. Robertson, J.: Diamond-Like amorphous carbon. *Mater. Sci. Eng.* **R37**, 129–281 (2002)
9. Ferrari, A.C., Robertson, J.: Interpretation of Raman spectra of disordered and amorphous carbon. *Phys. Rev. B* **61**(20), 14095–14107 (2000)
10. Liu, Y., Meletis, E.I.: Evidence of graphitization of diamond-like carbon films during sliding wear. *J. Mater. Sci.* **32**(13), 3491–3495 (1997)
11. Liu, Y., Erdemir, A., Meletis, E.I.: A study of the wear mechanism of diamond-like carbon films. *Surf. Coat. Technol.* **82**(1–2), 48–56 (1996)